Powder Technology 286 (2015) 269–275

Contents lists available at ScienceDirect

Powder Technology

journal homepage: www.elsevier.com/locate/powtec

Effect of surfactant on the morphology of ZnO nanopowders and their application for photodegradation of rhodamine B

Jian Wang [a,b], Jinghai Yang [c,*], Xiuyan Li [c,*], Bo Feng [c], Bing Wei [c], Dandan Wang [a,b], Hongju Zhai [c], Hang Song [a]

[a] Changchun Institute of Optics, Fine Mechanics and Physics, Chinese Academy of Sciences, Changchun 130033, PR China
[b] University of Chinese Academy of Sciences, Beijing 100049, PR China
[c] Key Laboratory of Functional Materials Physics and Chemistry of the Ministry of Education, Jilin Normal University, Siping 136000, Jilin, China

ARTICLE INFO

Article history:
Received 31 December 2014
Received in revised form 31 July 2015
Accepted 18 August 2015
Available online 21 August 2015

Keywords:
ZnO
Morphology
Growth mechanism
Photocatalytic property

ABSTRACT

ZnO nanopowders with different morphologies were successfully synthesized via hydrothermal method. By using different surfactants and controlling the concentration of surfactant in the reaction mixture, ZnO nanoparticles and nanoplates were obtained at 160 °C. The analysis of photoluminescence spectra shows that there exist more oxygen vacancies in the samples with small particle size and rough surface. The as prepared samples are used as photocatalysts for the rhodamine B (RhB) photodegradation, and the results show that ZnO with small particle size is more active for the photocatalytic process. This is attributed to the fact that the smaller particles have larger BET surface area and contain more surface oxygen vacancies, which are considered as stimulative for catalyzing the RhB reaction. The results suggest a positive relationship among particle size, oxygen vacancies and photocatalytic activity for RhB.

1. Introduction

Since environmental pollution has exceeded the limit of natural self-cleaning ability [1,2], semiconductor-based photocatalytic processes have attracted intense interest as an effective way of purifying contaminants [3–6]. Among the various semiconductors, ZnO, with a direct wide bandgap (Eg = 3.37 eV), is of special importance for the photocatalysis reaction [7,8], which can be utilized for the degradation of organic pollutants [4–6].

Because the photocatalytic reaction occurs at the interface between catalyst surfaces and organic pollutants [9], the photocatalytic activity of ZnO is strongly dependent on its morphology. Scientists have made great efforts in controlling the morphology of ZnO. Previous studies on the growth habits of ZnO under hydrothermal conditions have established that precursor, temperature, concentration, pH and using surfactants are all influencing factors on the resulting particle size and morphology [10–14].

Among these factors, surfactants play important roles in determining the different growth behaviors of ZnO [14,15]. The crystal growth habit can be modified by selective adsorption of surfactants on the planes of the polar crystals. Some surfactants have been introduced into the hydrothermal reactions to control the shape of ZnO. For example, specific novel ZnO morphology of layer-built spherical particles was prepared by a facile solution route in the presence of cetyltrimethylammonium chloride (CTAC) [16]. ZnO twin-spheres were synthesized on a large scale using a two-phase solution method in the presence of the water-soluble sodium bis (2-ethylhexyl) sulfosuccinate (AOT) [13]. However, there are still lots of unanswered questions about the effects of different surfactants on ZnO growth.

In addition, the introduction of surfactants can also bring great influence on the concentration of oxygen vacancies of ZnO [17]. According to the published work, the concentration of oxygen vacancies was one important factor to determine the photocatalytic performance of ZnO [18,19]. Surface oxygen vacancies always act as the photogenerated electron traps and the adsorption sites, in which the electron can transfer to the adsorbed sites, thus prevent the recombination of photoinduced electron-hole pairs, resulting in the enhancement of the photocatalytic activity.

In this work, ZnO with various morphologies was synthesized via a facile hydrothermal process under the assistance of different surfactants. Growth mechanism of the various ZnO morphologies was discussed. The effects of ZnO particle size and surface oxygen vacancies on the catalytic activity were investigated by RhB photodegradation.

2. Experimental

2.1. Materials

All reagents (including zinc nitrate hexahydrate ($Zn(NO_3)_2 \cdot 6H_2O$), sodium hydroxide (NaOH), cetyl trimethyl ammonium bromide (CTAB), polyethylene glycol-400 (PEG-400), and rhodamine B (RhB)) used in the experiments were of analytical grade (purchased from

* Corresponding authors.
E-mail addresses: jhyang1@jlnu.edu.cn (J. Yang), lixiuyan@126.com (X. Li).

http://dx.doi.org/10.1016/j.powtec.2015.08.030
0032-5910/

Table 1
Experimental condition of all samples.

ZnO nanopowders	$Zn(NO_3)_2 \cdot 6H_2O$ concentration (M)	NaOH concentration (M)	CTAB (M)	PEG-400 (ml/l)
Sample 1#	0.1	0.2	–	–
Sample 2#	0.1	0.2	0.01	–
Sample 3#	0.1	0.2	0.5	–
Sample 4#	0.1	0.2	–	40
Sample 5#	0.1	0.2	–	200

Sinopharm Chemical Reagent Co., Ltd.) and used without further purification.

2.2. Synthesis

In a typical procedure for preparing sample 1#, $Zn(NO_3)_2 \cdot 6H_2O$ was dissolved in deionized water. Subsequently, the appropriate dosage of NaOH solution in deionized water was added to the Zn precursor solution. This mixed solution was stirred for 10 min and then transferred to a Teflon-lined stainless steel autoclave and was thermally treated at 160 °C for 5 h. After cooling to room temperature, the white precipitate was washed with deionized water and ethanol several times and dried in an oven at 80 °C for 12 h to remove the solvent. For other ZnO nanopowders, the only change in the experimental condition is that the appropriate dosage of surfactant was dissolved with $Zn(NO_3)_2 \cdot 6H_2O$ when preparing Zn precursor solution. The following steps are the same with the procedure for preparing sample 1#. Experimental conditions for all samples are summarized in Table. 1.

2.3. Characterization

The crystallinity and phase purity of the products were characterized by using X-ray diffraction (XRD, MAC Science, MXP18, Japan). The morphologies and structures of the as-prepared nanopowders were analyzed by field emission scanning electron microscopy (FE-SEM, XL30ESEM-FEG and Hitachi S-4800) and transition electron microscopy (TEM, JEOL JEM-2010HR). N_2 adsorption isotherms were measured using an AUTOSORB-IQ (Quantachrome Instruments, USA). The photoluminescence spectrum was recorded at room temperature in a spectral range of 330 to 750 nm using a He–Cd laser with a wavelength of 325 nm as the excitation source. UV–vis absorption spectra were acquired with an UV–vis spectrophotometer (UV-5800PC, Shanghai Metash Instruments Co., Ltd.). The total organic carbon (TOC) was analyzed using vario TOC analyzer (vario TOC, Elementar, Germany).

2.4. Photocatalytic activity measurements

The photocatalytic activity measurement is as follows: the reaction system containing RhB aqueous solutions (7 mg/l) and the as-synthesized products were magnetically stirred thoroughly in the dark until reaching the adsorption equilibrium of RhB on catalyst before exposure to UV irradiation providing a 250 W high-pressure Hg lamp (centered at 365 nm). After different irradiation intervals, the solution concentration of RhB was analyzed by an UV–vis spectrophotometer at room temperature. The degradation efficiency of RhB was calculated from the following expression: the RhB degradation efficiency (%) $= (C_0 - C) / C_0 \times 100\%$, where C_0 and C are the concentrations of RhB before and after UV irradiation, respectively.

3. Results and discussion

3.1. Morphology and structure

Fig. 1 presents the SEM images of the as-prepared ZnO nanopowders. Five ZnO samples with different morphologies were obtained by changing the kind and dosage of surfactant. Fig. 1a shows the SEM image of ZnO hexagonal nanoplatforms (sample 1#) synthesized from the reaction without any surfactant. The average diameter and thickness of these nanopowders are about 230 and 200 nm, respectively. Fig. 1b shows the SEM image of sample 2#, synthesized from the reaction with 0.01 M CTAB acting as surfactant in the reaction solution. The morphology of ZnO nanopowders converted to plate-like nanostructures. The average lateral dimension and thickness of these nanopowders are 290 and 44 nm, respectively. If the dosage of CTAB was added to 0.5 M, ZnO nanoplates became bigger (sample 3#, Fig. 1c). The average lateral dimension and thickness of the nanoplates are approximately 350 and 50 nm, respectively. Fig. 1d shows the SEM image of the products (sample 4#) synthesized from the reaction with 40 ml/l PEG-400 serving as surfactant in the reaction solution. Sample 4# had a similar morphology with sample 1#, but the surface of sample 4# was not smooth and intact. The average diameter of these nanopowders is 150 nm. If the concentration of PEG-400 was added to

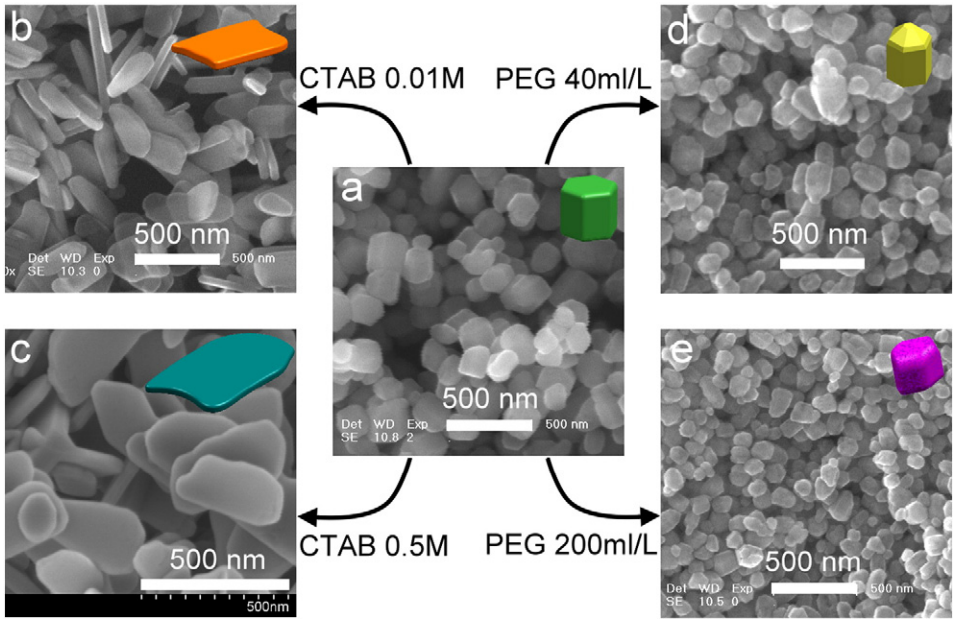

Fig. 1. SEM images of (a) samples 1#, (b) 2#, (c) 3#, (d) 4# and (e) 5#. Each inset shows a schematic model of each sample.

200 ml/l, ZnO nanoparticles became smaller (sample 5#, Fig. 1e). The average diameter of these nanopowders is 115 nm. Surfactants changed morphology of ZnO and we want to know if the crystalline type was also changed.

Particle size has great influence on the BET surface areas of nanomaterials. Without pores, particles with small size always have large BET surface areas. In this research, based on the N_2 adsorption isotherms (Fig. 2a) the BET specific surface areas of ZnO nanopowders were calculated using the Brunauer–Emmett–Teller (BET) method and the result is presented in Fig. 2b. Sample 5# whose particle size is the smallest has the largest BET surface area (13.39 m^2/g) among the as prepared nanopowders. The BET surface area decreases in turn for the ZnO nanopowders: 5# > 4# > 1# > 2# > 3#.

The crystal structures of as-prepared ZnO nanopowders were investigated by X-ray diffraction (XRD). Fig. 3 displays the XRD patterns of ZnO nanopowders with different morphologies. All the XRD patterns can be indexed as the pure hexagonal wurtzite ZnO nanostructure (JCPDS card, no. 36-1451). Because no diffraction peaks are observed from other impurities in the XRD patterns, it can be concluded that pure hexagonal-phase ZnO nanostructures are synthesized through this fast and simple hydrothermal method.

The crystalline natures of ZnO nanopowders (samples 1#, 3#, and 5#) were also investigated by using TEM. Fig. 4a1 shows the TEM image of sample 1#. The HRTEM image (Fig. 4a2) indicates that the structure is highly crystalline with a lattice spacing of 0.28 nm, which corresponded to the distance between the {10–10} planes in the ZnO crystal lattice. The SAED pattern laid on the [0001] zone axes and the sharp spots indicates the single crystalline nature of the structure (Fig. 4a3). Fig. 4b1 shows the TEM image of sample 3# obtained from the reaction with 0.5 M CTAB acting as surfactant in the reaction solution. The HRTEM image (Fig. 4b2) shows that the sample was highly crystalline with a lattice spacing of 0.26 nm, corresponding to the distance between the (0002) planes in the ZnO crystal lattice. The SAED pattern of the nanostructure revealed that it was single-crystalline (Fig. 4b3). Fig. 4c1 shows the TEM image of sample 5# synthesized from the reaction with 40 ml/l PEG-400 serving as surfactant in the reaction solution. The HRTEM image (Fig. 4c2) shows that the nanostructure was highly crystalline with a lattice spacing of 0.26 nm, corresponding to the distance between the (0002) planes in the ZnO crystal lattice. The SAED pattern of the nanostructure showed that the sample was also single-crystalline (Fig. 4c3).

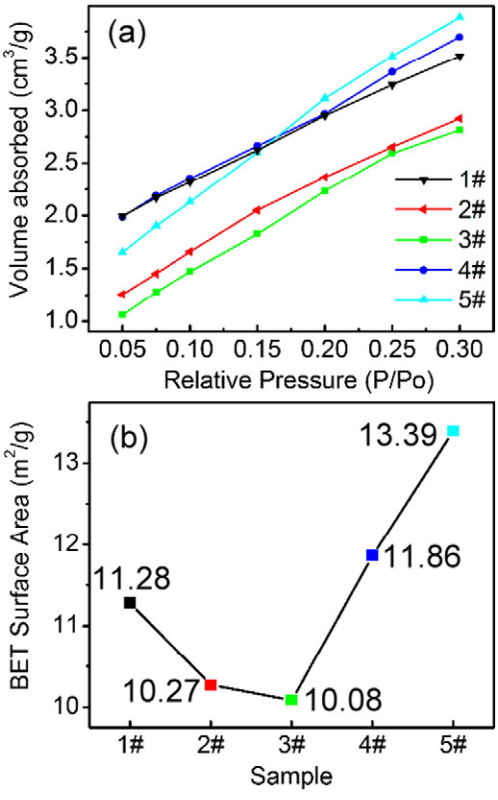

Fig. 2. N_2 sorption isotherms (a) and BET special surface (b) of all samples.

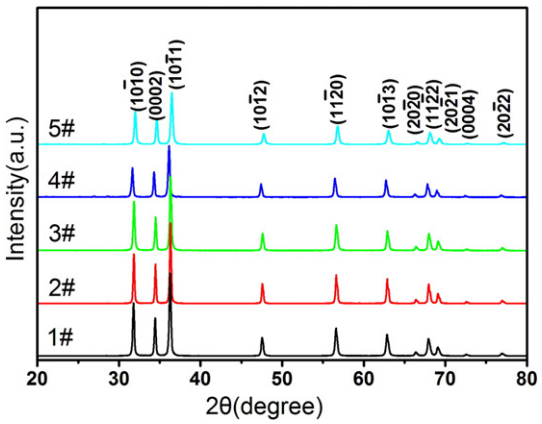

Fig. 3. XRD patterns of ZnO nanopowders.

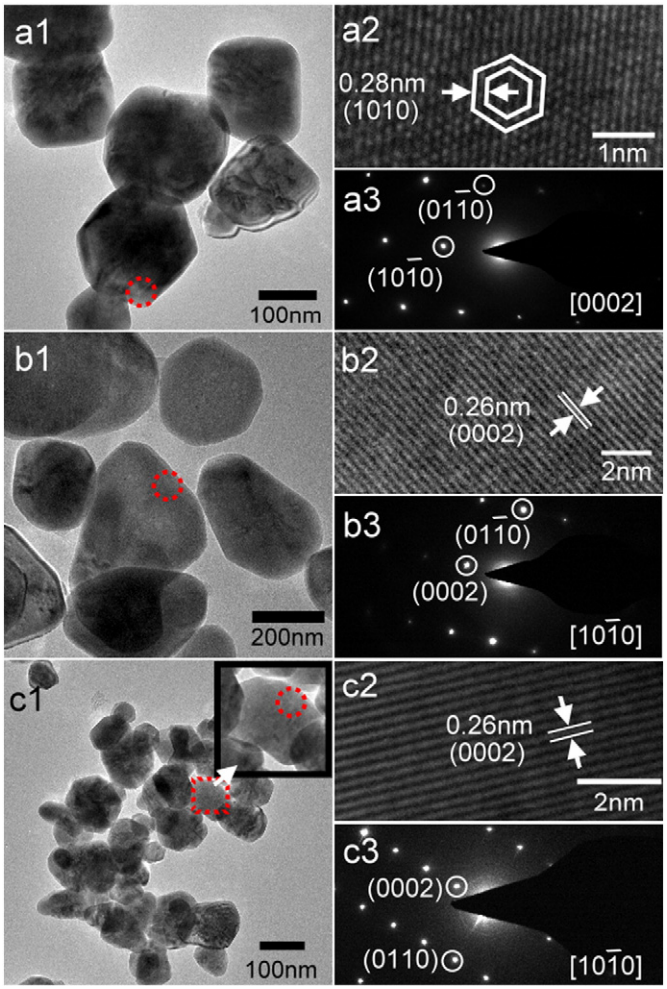

Fig. 4. (a1) TEM image of sample 1#; (a2) HR-TEM image and (a3) SAED pattern of the area indicated by the circle in (a1); (b1) TEM image of sample 3#; (b2) HR-TEM image and (b3) SAED pattern of the area indicated by the circle in (b1); (c1) TEM image of sample 5#; (c2) HR-TEM image and (c3) SAED pattern of the area indicated by the circle in (c1).

3.2. Growth mechanism

To understand the growth mechanism is indispensable in order to control and design tailored nanostructures. Based on the above experimental results, the growth mechanisms of ZnO nanopowders with different morphologies are proposed. In order to give a visual explanation, schematic illustration of growth mechanisms for ZnO nanopowders with different morphologies was displayed in Fig. 5.

The growth habit and morphology of the crystal depend on the relative growth rate of the different faces of the crystal [20–22]. Fig. 5a shows the schematic diagram of sample 1# which was prepared without any surfactants. The growth rate along the c axis should be a little higher than or at least equal to that along the radial axis, that is, V[0001] ≥ V[011-0]. This keeps the rod very uniform, well-faceted, and with both terminations flat.

The addition of surfactant in the reaction solution will induce changes in the kinetic parameters which can change the morphology. When the cation surfactant CTAB was introduced into the reaction system the surface tension of the solution was reduced and it will lower the energy needed to form a new phase. As we know, the growth unit of ZnO crystal is $[Zn(OH)_4]^{2-}$ in aqueous solutions, therefore, ion-pairs between CTA^+ and $[Zn(OH)_4]^{2-}$ could come into being through electrostatic interaction. During the hydrothermal reaction, CTAB plays a role as template and medium to transport the growth unit $[Zn(OH)_4]^{2-}$. According to the internal structure and growth habit of ZnO crystal, ZnO has the behavior of preferred growth along the c-axis [23]. These growth units combine with each other and decompose into ZnO nuclei simultaneously, which aggregate into ZnO nanorods. Meanwhile ZnO nanorods tend to conglomerate to form the structure of two dimensional nanoplate in order to lower the surface potential. The whole process can be clearly illustrated in Fig. 5b. When the dosage of CTAB was increased to 0.5 M, the size of ZnO nanoplate increased. That means more ZnO nanorods conglomerated together, as illustrated in Fig. 5c.

The morphology of ZnO nanopowders would look very different when the surfactant was replaced by a nonionic surfactant-PEG-400 (Fig. 1d and e). Along with the introduction of PEG-400 into hydrothermal system, the particle size decreased and surfaces of these particles became rough. This phenomenon might attribute to the restricting effect of the surfactant molecules present at the interface embracing the crystals and controlling their excess growth. With appropriate amounts of PEG-400 in the reaction solution, the additive molecules adsorb on the surfaces of ZnO nuclei during its growth process, including the face in the (0001) direction. Therefore, the active sites were covered and the growth of the crystals in all directions was restricted. The adsorption induced the formation of small ZnO nanoparticles with imperfect crystal faces, as illustrated in Fig. 5d. More PEG-400 molecules adsorbed on ZnO nuclei surfaces with 200 ml/l of PEG-400 in the reaction solution. Then the effect of PEG-400 molecules on the control of the crystal growth became stronger. Thus, nanoparticles with smaller mean particle sizes were obtained, as illustrated in Fig. 5e.

3.3. Optical properties and photocatalytic activities

PL spectra of as-synthesized ZnO nanopowders with different morphologies are presented in Fig. 6. On the whole, the room temperature PL spectra of all samples show similar features. There appeared one sharp UV emission band at about 380 nm, generally assigned as a near-band-edge (NBE) emission band, and another broad deep-level emission (DLE) band extending from 450 to 650 nm. The UV emission band ascribes to the free recombination of excitons. Such emission is in correspondence with the emission band reported in the literature [24,25]. The DLE emission has been associated to single ionized oxygen vacancies, oxygen antisites, zinc vacancies, and oxygen deficiency [26–29]. The green emission, which acts as the main ingredients among DLE emission for these samples, comes from the recombination of electrons in singly occupied oxygen vacancies with photoexcited holes [30,31]. Based on the above explanation, the relative density of the oxygen vacancies can be estimated by comparing the ratio of intensity of visible emission and UV emission (I_{Vis}/I_{UV}), and the higher I_{Vis}/I_{UV} ratio indicates the higher concentration of oxygen vacancies. So according to the inset of Fig. 6 the concentration of oxygen vacancies varies with different ZnO nanopowders showing the following order: 5# > 4# > 1# > 2# > 3#.

To compare the UV–vis absorb ability of the as prepared ZnO nanopowders, the UV–vis absorption spectra of ZnO nanopowders with different morphologies were shown in Fig. 7a. Sample 5# shows enhanced UV–vis absorption almost in the whole wavelength range

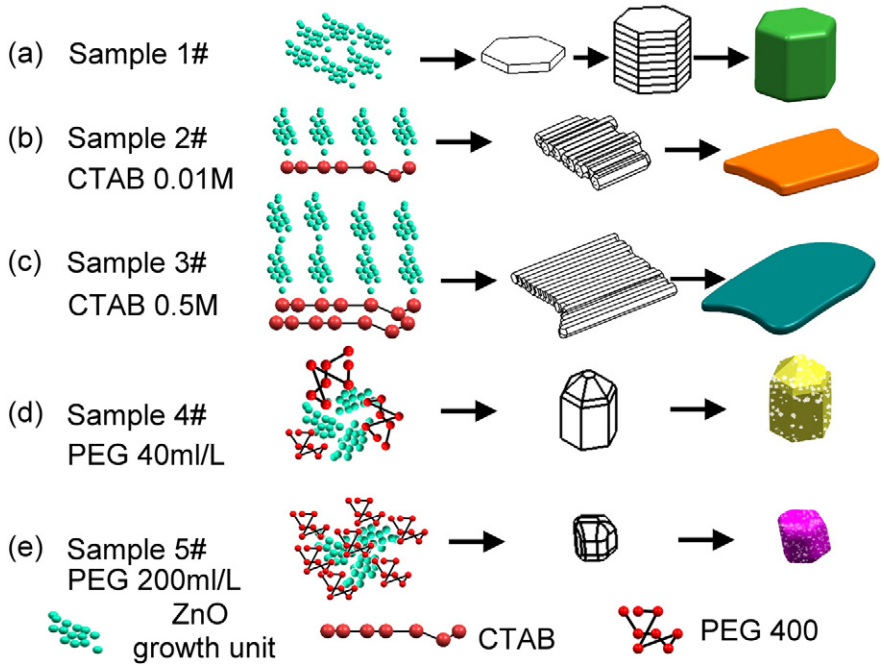

Fig. 5. Schematic illustration of growth mechanism for ZnO nanopowders with different morphologies.

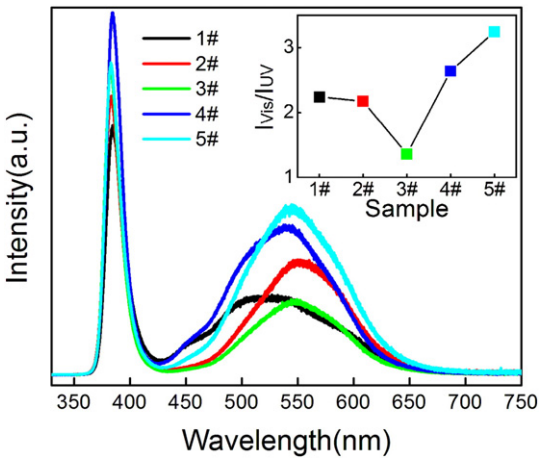

Fig. 6. PL spectra of all samples.

compared with others. On the contrary, sample 3# shows weaker absorption especially in UV range.

By using the Urbach model, band gaps of as prepared ZnO can be estimated as [32]

$$\alpha = \frac{A(h\nu - Eg)^n}{h\nu}$$

where A is a constant related to the mass of electron-hole pairs and the refractive index. As a direct band gap semiconductor, the value of A for ZnO is equal to 1/2. The curve of $(\alpha h\nu)^2$ versus $h\nu$ (photon energy) (Fig. 7b) was utilized to estimate the band gap of samples 1#, 3# and 5#. The calculated energy gaps for samples 1#, 3# and 5# are about 3.25, 3.31 and 3.01 eV in accordance with the previous reports. The difference in band gap might attribute to the content of oxygen vacancies. Wang et al. reported that when the concentration of oxygen vacancies is increased, the impurity states become more delocalized and overlap with the valence band edge, resulting to the band gap narrowing [19].

The results of the RhB degradation that used different ZnO photocatalysts are shown in Fig. 8. Without any catalyst, only a slow decrease in the concentration of RhB is detected (pink curve in Fig. 8a). The addition of catalysts leads to obvious degradation of RhB, and the photocatalytic activity depends on the morphology. Sample 5# showed the highest photocatalytic activity among the as prepared ZnO nanopowders and it can eliminate all RhB in the solution after 30 min UV irradiation (cyan curve in Fig. 8a). The activity decreases in turn for the as synthesized ZnO nanopowders: 5# > 4# > 1# > 2# > 3#. The first order kinetic equation $\ln(C_0/C) = kt$ is used to fit the experimental data in Fig. 8b, where k is the apparent rate constant. The k values obtained from Fig. 8b are 0.040, 0.030, 0.019, 0.072 and 0.132 min^{-1} in the presence of sample 1#–5#, respectively.

The total organic carbon (TOC) removal efficiency actually presents the true mineralization credibility of a photocatalyst. The time scale TOC removal of RhB dye is shown in Fig. 9. Compared with Fig. 8a, mineralization (TOC removal) of RhB is slower than its degradation efficiency. That means that RhB cannot be degraded into the final product directly. There exists transitional product in the photocatalytic process. Hence, longer irradiation time was required to obtain high TOC removal efficiency.

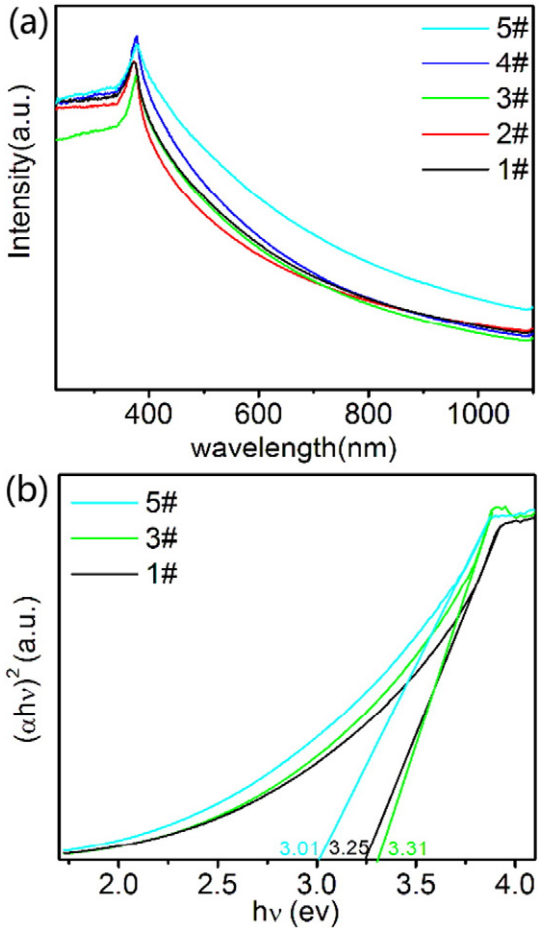

Fig. 7. UV–vis absorption spectra (a) and the plot of $(\alpha h\nu)^2$ versus $h\nu$ of ZnO nanopowders.

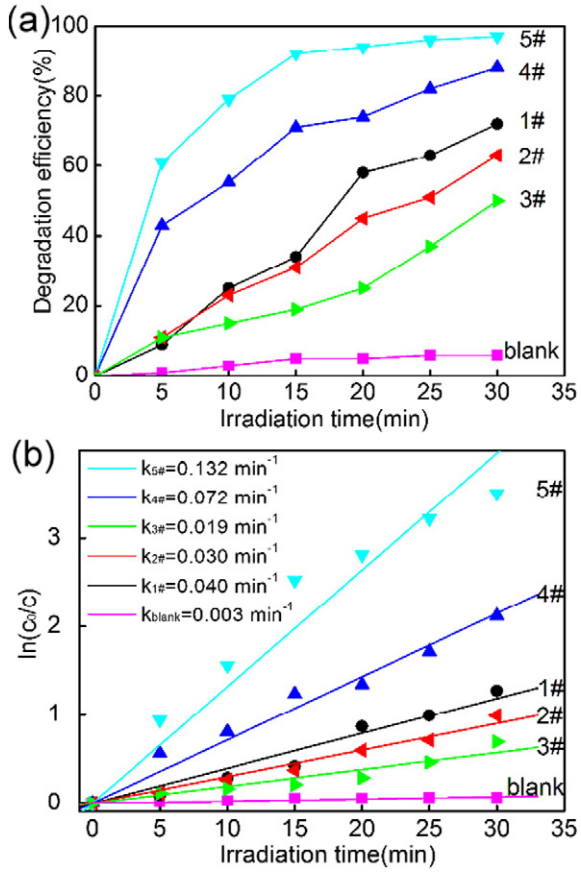

Fig. 8. (a) Degradation efficiency versus reaction time for all samples. (b) The relationship curves of the $\ln(C_0/C)$ versus reaction time for the ZnO photocatalysts.

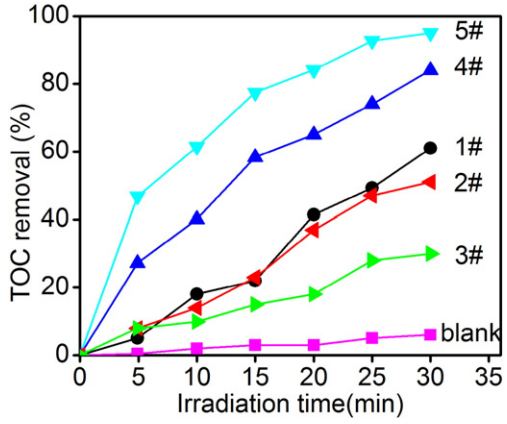

Fig. 9. The TOC removal profile of all samples.

Photocatalysis reaction is a complicated process, and the activity of the catalyst is influenced by many factors. The particle size is vitally important for the activity of oxide catalysts in photocatalytic reactions. According to the BET test shown in Fig. 2 we can conclude that small ZnO particles have large specific surface areas. A high specific surface area has a beneficial effect on the activity for catalysts because it can provide more chance for the contact between photocatalysts and contaminant. In this research, sample 5# has the smallest size, the largest BET surface area performed best in RhB photodegradation process.

In addition, oxygen vacancies are also important to determine the photocatalytic activity of ZnO photocatalysts [19,33,34]. It is well-known that oxygen vacancies can act as electron donors and have a contribution to enhance the donor density of semiconductor [35,36]. With the increase of donor density, charge transport in ZnO could be improved. The Fermi level of ZnO could also be shifted toward the conduction band [37]. This shift of the Fermi level can improve charge separation at ZnO/electrolyte interface. The surface oxygen vacancies can also absorb the oxygen species (such as O_2^-, OH^-) which could change into high-activity $\bullet O_2^-$ and $\bullet OH^-$, and they can accelerate the photocatalysis reaction [38–40]. Therefore, ZnO sample which contains more oxygen vacancies has higher catalytic activity for the RhB photodegradation reaction. According to the analysis result of PL test, sample 5# has the largest number of oxygen vacancies. That is one reason why sample 5# performed best in RhB photodegradation process.

4. Conclusions

We have synthesized ZnO nanopowders with different morphologies using a facile hydrothermal method by the assistance of surfactant. It has been shown that the introduction of CTAB can serve as template and obtain ZnO nanoplates in the hydrothermal reaction. When the PEG-400 was introduced as surfactant, the restricting effect of PEG-400 would make the particle small and rough in surface. In this study, samples with small size and rough surface have high concentration of surface oxygen vacancies. Further photocatalytic experiments confirm that ZnO samples with small particle sizes and high concentration of surface oxygen vacancies exhibit better photocatalytic activity in photodecomposition of RhB. This research may provide support for designing high photoactivity, environmental-friendly photocatalysts for environmental protection.

Acknowledgments

This work is supported by the National Programs for High Technology Research and Development of China (863) (item no. 2013AA032202), National Natural Science Foundation of China (grant nos. 61178074, 61378085 and 61308095), Program for the Development of Science and Technology of Jilin Province (item nos. 20130102004JC and 20140101205JC).

References

[1] B. Sovacool, P. Parenteau, M. Ramana, S. Valentine, M. Jacobson, M. Delucchi, M. Diesendorf, Comment on "prevented mortality and greenhouse gas emissions from historical and projected nuclear power", Environ. Sci. Technol. 47 (2013) 6715–6717.
[2] M.G. Zhou, Y.N. Liu, L.J. Wang, X.Y. Kuang, X.H. Xu, H.D. Kan, Particulate air pollution and mortality in a cohort of Chinese men, Environ. Pollut. 186 (2014) 1–6.
[3] C.C. Chen, W.H. Ma, J.C. Zhao, Semiconductor-mediated photodegradation of pollutants under visible-light irradiation, Chem. Soc. Rev. 39 (2010) 4206–4219.
[4] J. Xie, Y.T. Li, W. Zhao, L. Bian, Y. Wei, Simple fabrication and photocatalytic activity of ZnO particles with different morphologies, Powder Technol. 207 (2011) 140–144.
[5] R.Y. Hong, J.H. Li, L.L. Chen, D.Q. Liu, H.Z. Li, Y. Zheng, J. Ding, Synthesis, surface modification and photocatalytic property of ZnO nanoparticles, Powder Technol. 189 (2009) 426–432.
[6] T.G. Venkatesha, Y. Arthoba Nayaka, R. Viswanatha, C.C. Vidyasagar, B.K. Chethana, Electrochemical synthesis and photocatalytic behavior of flower shaped ZnO microstructures, Powder Technol. 225 (2012) 232–238.
[7] W. Xie, Y.Z. Li, W. Sun, J.C. Huang, H. Xie, X.J. Zhao, Surface modification of ZnO with Ag improves its photocatalytic efficiency and photostability, J. Photochem. Photobiol., A 216 (2010) 149–155.
[8] E. Yassıtepe, H.C. Yatmaz, C. Öztürk, K. Öztürk, C. Duran, Photocatalytic efficiency of ZnO plates in degradation of azo dye solutions, J. Photochem. Photobiol., A 198 (2008) 1–6.
[9] H. Park, Y. Park, W. Kim, W.Y. Choi, Surface modification of TiO_2 photocatalyst for environmental applications, J. Photochem. Photobiol. C 15 (2013) 1–20.
[10] W.W. Lee, J. Yi, S.B. Kim, Y.H. Kim, H.G. Park, W.I. Park, Morphology-controlled three-dimensional nanoarchitectures produced by exploiting vertical and in-plane crystallographic orientations in hydrothermal ZnO crystals, Cryst. Growth Des. 11 (2011) 4927–4932.
[11] M. Søndergaard, E.D. Bøjesen, M. Christensen, B.B. Iversen, Size and morphology dependence of ZnO nanoparticles synthesized by a fast continuous flow hydrothermal method, Cryst. Growth Des. 11 (2011) 4027–4033.
[12] S. Suwanboon, S. Klubnuan, N. Jantha, P. Amornpitoksuk, P. Bangrak, Influence of alkaline solutions on morphology of ZnO prepared by hydrothermal method for using as photocatalyst and bactericidal agent, Mater. Lett. 115 (2014) 275–278.
[13] F. Li, F.L. Gong, Y.H. Xiao, A.Q. Zhang, J.H. Zhao, S.M. Fang, D.Z. Jia, ZnO twin-spheres exposed in (001) facets: stepwise self-assembly growth and anisotropic blue emission, ACS Nano 12 (2013) 10482–10491.
[14] J.P. Du, R.H. Zhao, S. Chen, H.Y. Wang, J.P. Li, Z.P. Zhu, Self-assembly of gridlike zinc oxide lamellae for chemical-sensing applications, ACS Appl. Mater. Interfaces 7 (2015) 5870–5878.
[15] X.L. Zhang, R. Qiao, R. Qiu, J. Chang Kim, Y.S. Kang, Fabrication of hierarchical ZnO nanostructures via a surfactant-directed process, Cryst. Growth Des. 9 (2009) 2906–2910.
[16] E. Hosono, T. Tokunaga, S. Ueno, Y. Oaki, H. Imai, H.S. Zhou, S. Fujihara, Crystal-growth process of single-crystal-like mesoporous ZnO through a competitive reaction in solution, Cryst. Growth Des. 12 (2012) 2923–2931.
[17] H. Usui, Y. Shimizu, T. Sasaki, N. Koshizaki, Photoluminescence of ZnO nanoparticles prepared by laser ablation in different surfactant solutions, J. Phys. Chem. B 109 (2005) 120–124.
[18] C. Wang, D. Wu, P.F. Wang, Y.H. Ao, J. Hou, J. Qian, Effect of oxygen vacancy on enhanced photocatalytic activity of reduced ZnO nanorod arrays, Appl. Surf. Sci. 325 (2015) 112–116.
[19] J.P. Wang, Z.Y. Wang, B.B. Huang, Y.D. Ma, Y.Y. Liu, X.Y. Qin, X.Y. Zhang, Y. Dai, Oxygen vacancy induced band-gap narrowing and enhanced visible light photocatalytic activity of ZnO, ACS Appl. Mater. Interfaces 4 (2012) 4024–4030.
[20] H.G. Yang, C.H. Sun, S.Z. Qiao, J. Zou, G. Liu, S.C. Smith, H.M. Cheng, G.Q. Lu, Anatase TiO_2 single crystals with a large percentage of reactive facets, Nature 453 (2008) 638–641.
[21] R. Benages-Vilau, M. Rubbo, T. Calvet, M.À. Cuevas-Diarte, D. Aquilano, Growth kinetics of the {104} faces of nitratine ($NaNO_3$), Cryst. Growth Des. 13 (2013) 3419–3428.
[22] A.K. Zak, W.H.A. Majid, H.Z. Wang, R. Yousefi, A.M. Golsheikh, Z.F. Ren, Sonochemical synthesis of hierarchical ZnO nanostructures, Ultrason. Sonochem. 20 (2013) 395–400.
[23] W.J. Li, E.W. Shi, W.Z. Zhong, Z.W. Yin, Growth mechanism and growth habit of oxide crystals, J. Cryst. Growth 203 (1999) 186–196.
[24] R. Yousefi, A.K. Zak, M.R. Mahmoudian, Growth and characterization of Cl-doped ZnO hexagonal nanodisks, J. Solid State Chem. 184 (2011) 2678–2682.
[25] R. Yousefi, A.K. Zak, F.J. Sheini, Growth, X-ray peak broadening studies, and optical properties of Mg-doped ZnO nanoparticles, Mater. Sci. Semicond. Process. 16 (2013) 771–777.
[26] K.H. Tam, C.K. Cheung, Y.H. Leung, A.B. Djurisic, C.C. Ling, C.D. Beling, S. Fung, W.M. Kwok, W.K. Chan, D.L. Philips, L. Ding, W.K. Ge, Defects in ZnO nanorods prepared by a hydrothermal method, J. Phys. Chem. B 110 (2006) 20865–20871.
[27] S.A. Studenikin, N. Golego, M. Cocivera, Fabrication of green and orange photoluminescent, undoped ZnO films using spray pyrolysis, J. Appl. Phys. 84 (1998) 2287.
[28] D. Li, Y.H. Leung, A.B. Djurisic, Z.T. Liu, M.H. Xie, S.L. Shi, S.J. Xu, W.K. Chan, Different origins of visible luminescence in ZnO nanostructures fabricated by the chemical and evaporation methods, Appl. Phys. Lett. 85 (2004) 1601.

[29] W.M. Kwok, A.B. Djurisic, Y.H. Leung, W.K. Chan, D.L. Phillips, Time-resolved photoluminescence from ZnO nanostructures, Appl. Phys. Lett. 87 (2005) 223111.
[30] H. Usui, Influence of surfactant micelles on morphology and photoluminescence of zinc oxide nanorods prepared by one-step chemical synthesis in aqueous solution, J. Phys. Chem. C 111 (2007) 9060–9065.
[31] D. Zhao, X.X. Zhang, H.B. Dong, L.J. Yang, Q.S. Zeng, J.Z. Li, L. Cai, X. Zhang, P.S. Luan, Q. Zhang, M. Tu, S. Wang, W.Y. Zhou, S.S. Xie, Surface modification effect on photoluminescence of individual ZnO nanorods with different diameters, Nanoscale 5 (2013) 4443–4448.
[32] W. Lee, S.K. Min, V. Dhas, S.B. Ogale, S.H. Han, Chemical bath deposition of CdS quantum dots on vertically aligned ZnO nanorods for quantum dots-sensitized solar cells, Electrochem. Commun. 11 (2009) 103–106.
[33] T.R. Gordon, M. Cargnello, T. Paik, F. Mangolini, R.T. Weber, P. Fornasiero, C.B. Murray, Nonaqueous synthesis of TiO_2 nanocrystals using TiF_4 to engineer morphology, oxygen vacancy concentration, and photocatalytic activity, J. Am. Chem. Soc. 134 (2012) 6751–6761.
[34] G.R. Li, T. Hu, G.L. Pan, T.Y. Yan, X.P. Gao, H.Y. Zhu, Morphology–function relationship of ZnO: polar planes, oxygen vacancies, and activity, J. Phys. Chem. C 112 (2008) 11859–11864.
[35] A. Naldoni, M. Allieta, S. Santangelo, M. Marelli, F. Fabbri, S. Cappelli, C.L. Bianchi, R. Psaro, V.D. Santo, Effect of nature and location of defects on bandgap narrowing in black TiO_2 nanoparticles, J. Am. Chem. Soc. 134 (2012) 7600–7603.
[36] A. Janotti, J.B. Varley, P. Rinke, N. Umezawa, G. Kresse, C.G. Van de Walle, Hybrid functional studies of the oxygen vacancy in TiO_2, Phys. Rev. B Condens. Matter 81 (2010) 085212.
[37] D.C. Cronemeyer, Infrared absorption of reduced rutile TiO_2 single crystals, Phys. Rev. 113 (1959) 1222–1226.
[38] H.M. Xiong, D.G. Shchukin, H. Mohwald, Y. Xu, Y.Y. Xia, Sonochemical synthesis of highly luminescent zinc oxide nanoparticles doped with magnesium(II), Angew. Chem. Int. Ed. 48 (2009) 2727–2731.
[39] Q.J. Xiang, J.G. Yu, P.K. Wong, Quantitative characterization of hydroxyl radicals produced by various photocatalysts, J. Colloid Interface Sci. 357 (2011) 163–167.
[40] Q.J. Xiang, J.G. Yu, W.G. Wang, M. Jaronie, Nitrogen self-doped nanosized TiO_2 sheets with exposed {001} facets for enhanced visible-light photocatalytic activity, Chem. Commun. 47 (2011) 6906–6908.